A chemo-mechanical model for nuclear morphology and stresses during cell transendothelial migration

X. Cao, E. Moeendarbary, P. Isermann, P. Davidson, X. Wang, M Chen, A. Burkart, J. Lammerding, R.D. Kamm, V. Shenoy

Abstract

It is now evident that the cell nucleus undergoes dramatic shape changes during important cellular processes such as cell transmigration through extracellular matrix and endothelium. Recent experimental data suggest that during cell transmigration the deformability of the nucleus could be a limiting factor, and the morphological and structural alterations that the nucleus encounters can perturb genomic organization that in turn influence cellular behavior. Despite its importance, a biophysical model that connects the experimentally observed nuclear morphological changes to the underlying biophysical factors during transmigration through small constrictions is still lacking. Here, we developed a universal chemo-mechanical model that describes nuclear strains and shapes and predicts thresholds for the rupture of the nuclear envelope and for the nuclear plastic deformation during transmigration through small constrictions. The model includes actin contraction and cytosolic back-pressure that squeeze the nucleus through constrictions and overcome the mechanical resistance from deformation of the nucleus and the constrictions. The nucleus is treated as an elastic shell encompassing a poroelastic material representing the nuclear envelope and inner nucleoplasm, respectively. Tuning the chemo-mechanical parameters of different components such as cell contractility, nuclear and matrix stiffnesses, our model predicts the lower bounds of constriction size for successful transmigration. Furthermore, treating the chromatin as a plastic material, our model faithfully reproduced the experimentally observed irreversible nuclear deformations following transmigration in lamin A/C deficient cells, while the wild–type cells show much less plastic deformation. Along with making testable predictions, which are in accord with our experiments and existing literature, our work provides a realistic framework to assess the biophysical modulators of nuclear deformation during cell transmigration.

Introduction

Tumor cell extravasation is one of the critical, and possibly rate-limiting, steps in the process by which cancer spreads to metastatic sites from a primary tumor (1, 2). While we know relatively little about the details of extravasation, recent *in vitro* studies have elucidated a process beginning with tumor cell arrest in the microcirculation and the formation of protrusions that reach across the endothelial monolayer, accompanied by polarization of tumor cell actin and activation of beta-1 integrins to generate firm adhesions (3, 4). This is rapidly followed by actomyosin contraction to generate the forces needed to pull the remaining cell body across the monolayer. Similarly, during invasion into tissues, tumor cells use actomyosin activity to squeeze through tight interstitial spaces (5). During these processes, the cell size, rheological properties and the geometric parameters associated with the extracellular environment dictate the maximal rate at which the cell can transmigrate and change its shape (6, 7). The nucleus, being the largest and the stiffest organelle within the cell, is a physical constraint to migration and may be a rate-limiting factor for cellular deformations during cell migration through 3-dimensional (3D) constrictions that are smaller or comparable to the nuclear cross section (8–10). On the other hand, since the nucleus houses the genetic machinery of the cell, changes in the nuclear morphology and

positioning within the cytoplasm during migration can influence the phenotypic profile of the cell (11, 12). For instance, it has been recently shown that in addition to the ability of cells to dramatically squeeze their nuclei to pass through small constrictions, cells utilize components of the ESCRT (endosomal sorting complexes required for transport) machinery to repair the concomitant damage to their nuclear envelope (NE) and DNA that occur during confined migration (13, 14).

In light of experimental discoveries that identified nuclear morphological changes and their implications for cellular behavior, progress has been made in quantifying mechanical and rheological properties of the nucleus (15, 16). Yet, how actomyosin-generated forces coordinate with geometric and mechanical parameters (such as the constrictions size, stiffness of the extracellular matrix and the nucleus) to modulate the nuclear morphology during cell passage through small openings remains poorly understood. Furthermore, despite the development of a variety of approaches that model mechanics of the whole cell (17–19), a mechanistic model to assess the ability of cells to pass through small constrictions and the role of nucleus and other biophysical parameters is still lacking.

To address these shortcomings, we developed a novel chemo-mechanical model that describes nuclear morphology during cell migration through deformable constrictions smaller than the size of the nucleus. Based on biophysical modulators of transmigration including actomyosin contractility, the geometric and mechanical properties of the opening, the nucleus and the extracellular matrix (ECM), our model estimates the stiffness-dependent actomyosin driving forces and the mechanical resistance encountered by the nucleus, to predict the chances of successful transmigration. By varying these biophysical factors, we computed the strain distribution within the nucleus at different stages of transmigration to elucidate the physical mechanisms behind nuclear envelope and DNA damage as well as the thresholds for plastic deformation of the nucleus. To verify our model, we simulated nuclear transmigration through an endothelial gap and also passage through rigid constrictions. Tuning our model parameters by comparison with experimental measurements, our framework provides a quantitative description of nuclear mechanics during transmigration of cancer cells across the endothelial monolayer and through rigid constrictions.

Materials and Methods
Model formulation
In order to understand the influence of both the intracellular and extracellular cues and the mechanical properties of the nucleus on cell transmigration, a cell with a spherical nucleus of radius r_n invading extracellular matrix (ECM) through a deformable gap smaller than the diameter of the nucleus (Fig. 1c) is considered. The nucleus is treated as a non-linear shell with shear modulus μ_s, simulating the nuclear envelope, filled with a soft poroelastic solid material

mimicking chromatin and other sub-nuclear structures (Fig. 1c, refer to Supplementary Information for details). Recent work has shown that nucleus is also viscoelastic, but the time scale of viscous relaxation is of the order of 10-300 sec (15, 16, 20, 21), which is an order of magnitude smaller than the time it takes the nucleus to pass through endothelial gaps/constrictions. Thus the elastic properties we use here are the moduli after the viscous effects have relaxed. To model the extracellular environment, a thin flexible layer with a hole or gap of radius r_g mimicking the endothelium (or a constriction in a microfluidic device) and a deformable ECM placed on the other side of the endothelium are introduced (Fig. 1c). The endothelium (or constriction) and the ECM are treated as compressible neo-Hookean hyperelastic materials to capture the mechanical response (refer to Supplementary Information for details).

The actomyosin contraction at the front of the cell provides the driving force for transmigration. Cell can adjust its contractility by controlling myosin motor recruitment through variety of signaling pathways, such as Rho-ROCK and Ca (Fig. 1d, refer to Supplementary Information for details). Here we applied our recently published model (22) to introduce the stiffness-dependent recruitment of the contractile machinery (Fig. 1e, refer to Supplementary Information for detailed descriptions) that accounts for the influence of both intracellular (for example, signal pathways) and extracellular cues (ECM modulus and deformation). The resistance force during transmigration is calculated using the finite element method (FEM) to compute the deformations of the nucleus, endothelium and ECM. Transmigration is predicted to be successful if the resistance force is smaller than the actomyosin contractile force. The simulation steps are shown in Supplementary Fig. 1.

AFM
AFM microindentation measurements of gel and cell nucleus elasticity were performed using a JPK NanoWizard I (JPK Instruments) interfaced to an inverted optical microscope (IX81, Olympus). Cantilevers (MLCT, Bruker; nominal spring constants of 0.07 N m^{-1}) were modified by attaching beads (15 μm beads for cellular measurements and 50 μm for gel) using UV curing glue. Using the thermal noise method implemented in the AFM software (JPK SPM), the spring constants of the cantilevers were determined. Prior to measurements, the sensitivity of the cantilever was set by measuring the slope of the force-distance curves acquired on a glass-bottom petri dish. To determine the nucleus elasticity we applied force to the nuclear regions of the cell with large forces (> 9 nN) to create indentation depths > 2 μm that ensure significant deformation of the nucleus and thereby maximize the contribution of the nucleus to the measured elasticity (23). The tip of the cantilever was aligned over the regions above the cell nucleus using the optical microscope and indentation measurements were performed. Force-distance curves were acquired with an approach speed of 1 μm s^{-1} until reaching the maximum set force of 20 nN. Using a previously described method (24), we found the contact point, and subsequently calculated the indentation depth δ by subtracting the cantilever deflection d from the piezo translation z after

contact ($\delta = z - d$). The elastic moduli were extracted from the force-distance curves by fitting the contact portion of curves to a Hertz contact model between a spherical indenter and an infinite half-space (25).

Microfluidic device and NE rupture experiments

Details on the microfluidic device fabrication, cells used, and analysis for the chromatin deformation have been described previously (26). In brief, cells were plated in a microfluidic device made of polydimethylsiloxane (PDMS) and a glass slide, containing 5 µm tall migration channels with constrictions of 1 to 15 µm in width. Cells migrate along a chemotactic gradient, and nuclear deformation is observed by time-lapse imaging of fluorescently labeled histones. As decribed previously, nuclear envelope rupture was detected by monitoring the transient escape of GFP fused with a nuclear localization signal (NLS-GFP) from the nucleus into the cytoplasm and fluorescently labeled cytoplasmic DNA-binding protein (cGAS-RFP) that accumulates at newly exposed genomic DNA was used to monitor the sites of nuclear envelope rupture (14). Cells were generated by stable expression of fluorescent reporter proteins, i.e. NLS-GFP and cGAS-RFP, by lentiviral transduction. For confined migration experiments cells were loaded into a custom manufactured microfluidic device and imaged for 14 h on a temperature-controlled microscope. Image analysis was carried out in ZEN (Zeiss), Matlab (MathWorks) and ImageJ.

Results

During extravasation, the invading cancer cell sends protrusions between two adjacent endothelial cells, and creates a small opening within the endothelial layer (4). The actin rich protrusions at the front of the cell (the green region in Fig. 1a) adhere to and pass through the basement membrane, penetrating into the ECM. During transendothelial migration (TEM), the actomyosin-mediated contractile forces generated in the 'pre-invaded' part of cell and around the nucleus, push/pull the nucleus to pass through the endothelial gap. Similarly, as cells migrate through interstitial spaces, they have to move through confined spaces imposed by extracellular matrix fibers and surrounding cells (9). In order to understand the influence of both the intracellular and extracellular cues and the mechanical properties of the nucleus on cell transmigration, we consider the case of a cell with an initially spherical nucleus of radius r_n invading the ECM through the endothelial layer or, more generally a gap (of radius r_g) smaller than the radius of the nucleus (Fig. 1b and c). We adopted our recently developed chemo-mechanical model (22) to describe the stress-dependent actomyosin activity (Fig. 1e), which is mediated by mechanosensitive signaling pathways such as the Src-family kinases (SFK), rho-associated protein kinase (ROCK) and myosin light-chain kinase (MLCK), as shown in Fig. 1d. We first studied the mechanics of nuclear transmigration through deformable constrictions to mimic TEM and then explored cell passage through rigid constrictions, for example ones in microfluidic devices whose dimensions can be specified (26).
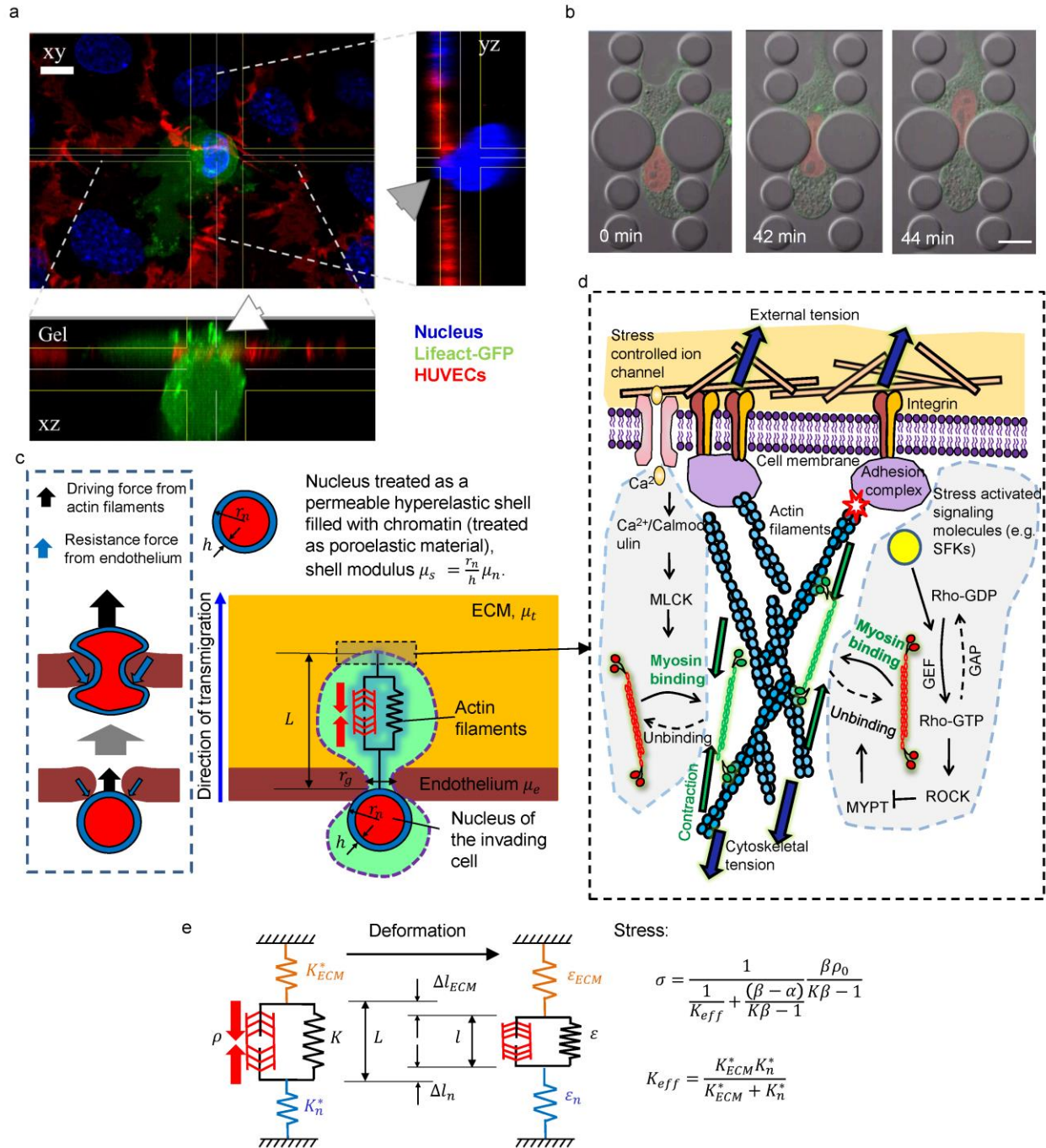
Figure 1: Computational model for tumor cell transmigration: (a) High resolution confocal z-stack of a cancer cell (Lifeact-GFP, MDA-MB-231, green) transmigrating through an endothelial monolayer (PECAM-1, HUVECs, red) cultured on a collagen gel. The nuclei were stained with Hoechst (blue). The white arrow indicates actin rich protrusions at the leading edge of the cancer cell entering the ECM. The gray arrow indicates the front of the cancer cell nucleus squeezing through the endothelial gap. Scale bar, 10 μm. (b) Representative time-lapse images of a fibroblast (NIH 3T3) expressing mCherry-Histone4 (red) and GFP-actin (green) migrating through a 3 μm-wide rigid constriction in a 5 μm-tall microfluidic device. Scale bar, 15 μm. (c) The nucleus is modeled as a permeable hyperelastic shell (representing NE) with modulus μ_s filled with

chromatin (modeled as a poroelastic material with modulus μ_c and Poisson's ratio in the range of 0.3~0.5 based on permeability). The parameters in the model are the shear modulus for the endothelium (μ_e), the ECM (μ_t) and the nucleus (μ_n); nuclear radius (r_n), endothelial gap size (r_g) and the average length of the actin filaments (L). The nuclear stiffness μ_n is mainly determined by the NE elasticity $\mu_s = (r_n/h)\mu_n$, $\mu_c = 0.1\mu_n$, where h is the thickness of the shell. (d) The driving force for transmigration is generated by stress-dependent contraction of actomyosin complex. The actomyosin activity is mediated by a variety of biochemical processes, such as the rho-ROCK and calcium mediated pathways (see Supplementary Information for details). (e) Schematic for the mechanical model of active contractile stress generation. The actomyosin contraction is modeled by a spring in parallel with an active contractile element, which ensures that stiffer ECMs will generate larger contractile stresses (see Supplementary Information for details).

ECM stiffness and gap size modulate nuclear transmigration

We employed Finite Element simulations to estimate the normalized resistance force (F^*) during each stage of nuclear transmigration (see Supplementary Information for details). While the nucleus enters the constriction, F^* increases monotonically as the nucleus advances, reaching a maximal resistance force (which we name the critical resistance force, F_c^*) at a critical position. Following this, the nucleus snaps through the opening, leading to a drop in the resistance force, which vanishes after complete nuclear escape (Supplementary Fig. 2a). To predict the driving force, we calculated the normalized actomyosin contractile forces (F_α^*) based on an actin contraction model (22) that relies on a mechano-chemical feedback parameter α, that accounts for the increase in contractility in response to tension in the actomyosin system (see Supplementary Information for details). Through myosin motor recruitment, the contractile force gradually reaches its maximum level to overcome the resistance force leading to successful transmigration, $F_\alpha^* \geq F_c^*$. α_c is defined as the critical mechano-chemical coupling parameter that is just sufficient for transmigration to occur ($F_\alpha^* = F_c^*$ at the critical position). At weak feedback levels ($\alpha < \alpha_c$), the cell is unable to build up enough driving force for the nucleus to pass through (Supplementary Fig. 2b, top two panels); while at higher feedback levels ($\alpha \geq \alpha_c$), the cell is able to generate the critical force required to snap through the gap (Supplementary Fig. 2b, bottom two panels).

Our model shows that the radii of the nucleus (r_n) and the endothelial gap (r_g), and the moduli of the endothelium (μ_e) and the nucleus (μ_n) are the main determinants of the resistance force F^*. Indeed, transmigration is difficult through small endothelial gaps (Fig. 2a) and a stiffer endothelium also impedes transmigration. Though the modulus of the ECM (μ_t) has little influence on the resistance force, it has a strong effect on the actomyosin contractile forces: at the same chemo-mechanical coupling level, softer ECM induce lower levels of cellular contractile force (22, 27, 28), which may not be sufficient for the cells to overcome the resistance force. Therefore, it is less likely for the cell to transmigrate when ECM is soft (Fig. 2b). On the other hand, a stiffer ECM often has smaller pores, which impose higher geometrical constraints on cell

movement. Therefore, although a cell encountering a stiff ECM can develop higher contractile forces, the chances of successful transmigration are still limited by the geometric constraints.

By varying the model parameters, we have predicted the normalized critical feedback strength (α_c/β, where β is chemo-mechanical coupling parameter related to motor engagement, see Supplementary Information for details) as a function of the radius of the endothelial constriction and the ECM modulus (Fig. 2c). The model predicts the physical limit for successful transmigration to be $r_g \sim 0.3 r_n$, corresponding to about 10% of the undeformed nuclear cross-sectional area, in excellent agreement with previous measurements (9) as shown in Supplementary Fig. 6. Our AFM measurements of the elastic properties of components of an extravasation monolayer assay show $\mu_t = 211 \pm 20$ Pa, $\mu_e = 588 \pm 200$ Pa, $\mu_n = 1150 \pm 420$ Pa (Supplementary Fig. 3). This, together with the geometrical parameters extracted from our system (Supplementary Fig. 3), implies that cancer cells have to overcome a resistance force of ~38 nN to successfully transmigrate through endothelial constrictions as small as 30% of the nucleus size, which is within the physiological range (29).

Lamin A/C level is one of the main determinants of the resistance forces
It has been shown that the levels of the nuclear envelope proteins lamin A and C (lamin A/C) determine the stiffness of the nucleus (21, 30–32), and lower levels of lamin A/C facilitate cell migration through tight spaces (8, 10, 33). We studied the influence of lamin A/C on transmigration by varying the modulus of the NE in our model (Supplementary Fig. 4). The critical resistance force linearly increases with increasing nuclear stiffness. Contractile driving force also increases with increase in the nuclear and ECM stiffness, but eventually reaches a plateau (Supplementary Fig. 4). Therefore, transmigration cannot occur due to the lack of sufficiently large contractile forces if cells have very stiff nuclei (wild-type cells) (29). For soft nuclei (e.g., lamin A/C-deficient cells), the resistance force is much smaller than the contractile force, implicating transmigration is much easier for these cells, but is accompanied by large nuclear deformations, consistent with recent measurements in microfluidic devices (26).

Contribution of the cytosolic back-pressure on transmigration
During transmigration, the nucleus can divide the cell into two parts with a pressure difference (Δp) between these parts created by the cortical membrane tension in the front and rear cytosolic compartments. For simplicity, we assume that the membrane tension is uniform and that the front and rear cytosol compartments are both spherical with radii r_f and r_r respectively (Fig. 2d). The pressure difference (rear - front) can be estimated as $\Delta p = 2\gamma(1/r_r - 1/r_f)$, where γ is the actin cortical tension. Recently it has been shown that the nucleus partitions the cytoplasm after the cell transports the majority of its cytosol to the front (3). As a result, $r_r < r_f$, and $\Delta p > 0$, indicating that membrane tension creates a positive pressure difference that pushes the nucleus from the back

to assist transmigration. To study the effect of membrane tension and back-pressure from the cytosol, we consider an extreme case in which the cell translocates almost all cytosol before nuclear transmigration, meaning $r_r \approx r_n$ and $r_f = 2.5r_n$, which is commonly seen in our experiments with very small gap sizes. To estimate the pressure difference, we consider a cortical actin tension of $\gamma = 2 \times 10^{-3} J/m^2$ based on a previous study (34). The additional driving force due to cytosolic pressure is $\Delta F = \Delta p \pi r_g'^2$, where r_g' is the endothelial gap radius in the current state (Fig. 2d). For a certain gap size and mechanical properties of different components, while the resistance force stays the same, the required active contractile force for successful transmigration can be smaller when considering this cytosolic back-pressure ($F_\alpha = F - \Delta F$). Therefore, cytosolic back-pressure from membrane tension promotes transmigration.
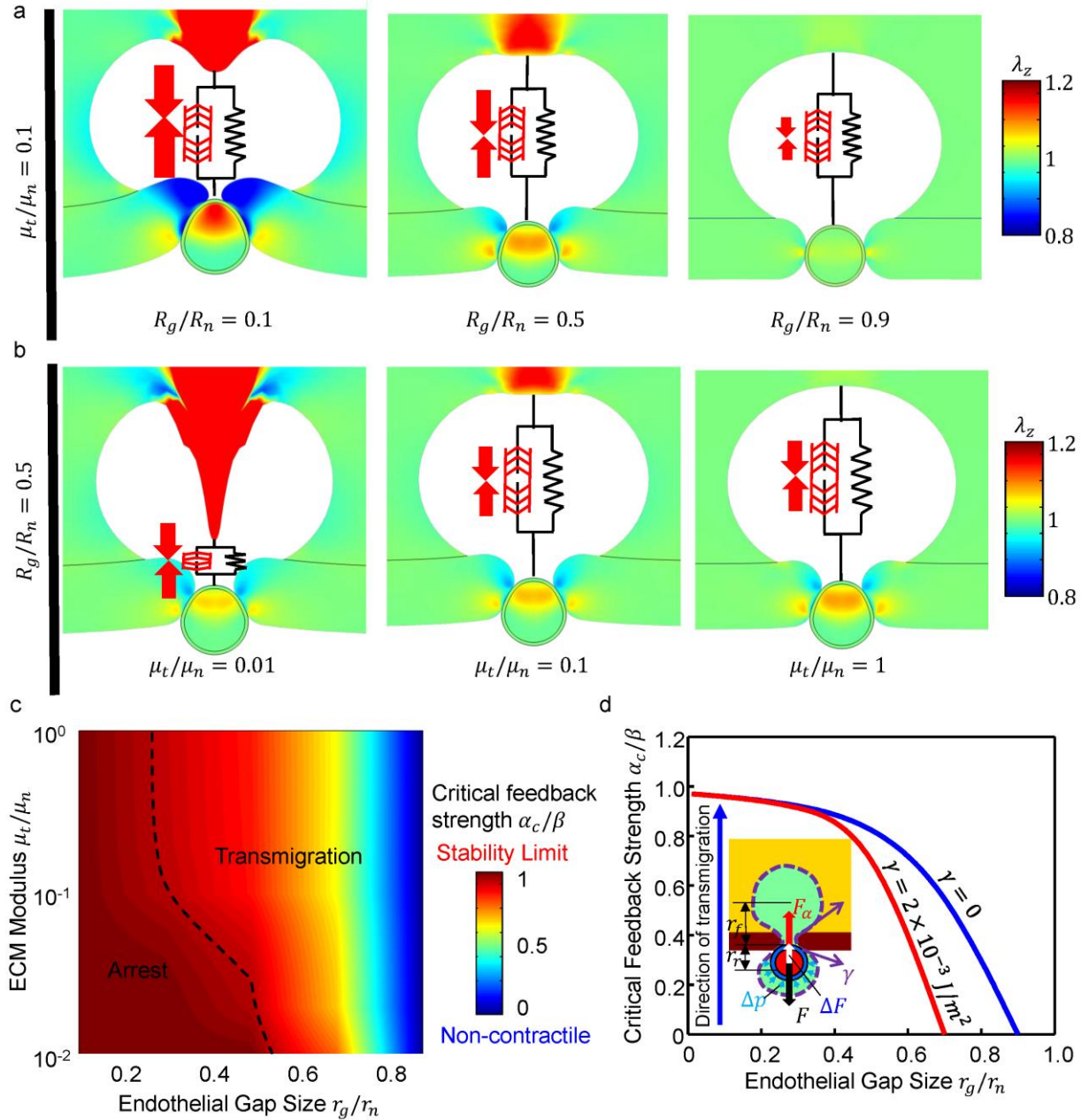
Figure 2: Influence of the endothelial gap size (r_g) and ECM modulus (μ_t) on transmigration: (a) As the gap size decreases (from right to left) the cell cannot transmigrate through the smaller gaps because of the increase in critical resistance force. (b) As the ECM stiffness decreases (from right to left) cells cannot transmigrate since they cannot build up sufficient contractile forces in soft ECMs. Colors in (a) and (b) indicate the stretches along the direction of invasion. (c) Critical feedback strength as a function of the ECM modulus and the endothelial gap size predicted by the model. The dashed line denotes the phase boundary for transmigration. On the right-hand side of the phase boundary, $\alpha_c/\beta < 0.87$ and the cells can pass through the gap. The model predicts the physical limit of $r_g \sim 0.3 r_n$ for successful transmigration, corresponding to ~10% of the undeformed nuclear cross-section, in excellent agreement with previous measurements (9) as shown in Supplementary Fig. 6. (d) Cytosolic pressure generated through cortical actomyosin

contractility can promote transmigration. Comparison between the critical feedback strength required for transmigration as a function of the endothelial gap size with (red) and without (blue) accounting for pressure exerted on the nucleus due to membrane tension. Model parameters are $K = 1$ kPa, $\rho_0 = 0.5$ kPa, $\beta = 2.77 \times 10^{-3}$ Pa, $\mu_n = 5$ kPa, $\mu_e = 1$ kPa, $\mu_t = 0.5$ kPa in (a), $r_g = 0.5 r_n$ in (b).

Effects of compressibility and NE permeability on nuclear volume change

The biochemical interactions of the nuclear proteins are dependent on the amount of accessible water that regulates the levels of pH, ionic strength and the concentration of different chemical species within the nucleus. We considered water displacement in and out of the nucleus (through pores), but also the redistribution of water within the nucleus as it is compressed locally. The structural organization and function of nuclear macromolecules rely on the physical and thermodynamic interactions between different nuclear components and the excluded volume effects of macromolecular crowding. The change in water concentration within the nucleus can be directly correlated to the nuclear volume change through:

$$c = c_{ref} + \frac{1}{\Omega}\frac{\Delta V}{V_0}$$

where c_{ref} is the water concentration in the reference state prior to transmigration and Ω is the volume per water molecule. Therefore, considering its implications on excluded volume effects as well as water concentration and redistribution, here we investigate the changes in nuclear volume during transmigration. We estimated the normalized nuclear volume change ($\Delta V/V_0$) as a function of the normalized nuclear position with respect to the gap (z^*) considering different constriction sizes. Our model predicts that the nucleus undergoes substantial shape change during transmigration leading to significant volume decrease (Fig. 3a and 3c). The experimental model confirmed the large variations in shape (Fig. 3b) but did not find significant changes in the nuclear volume (26), but accurate volume measurements are difficult to obtain even using high resolution 3-D confocal microscopy. In the case of relatively small gaps ($r_g = 0.5 r_n$) the predicted shape change and volume decrease (~24%) are dramatic, leading to significant fluid efflux that influences the water concentration and macromolecular crowding (Fig. 3c). For larger gaps, though the overall volume change is small (~13%, Fig. 3c) there is still large reduction (~20%, Fig. 3d) in localized fluid volume (dilatation) leading to decrease in the amount of accessible water locally.

We also investigated effects of decreasing the nucleus permeability thereby impeding fluid outflow and redistribution. To address effects of permeability, we considered changing the 'dry' Poisson ratio (Poisson ratio of solid phase in the poroelastic material). Considering values close to 0.5 for the dry Poisson ratio (set as 0.49) implicates almost non-permeable nuclear envelope with minimal chances of fluid outflow. In this case and as expected the overall volume changes (~1%) are significantly reduced compared to the permeable cases (Fig. 3c). A recent study showed that the nuclei of fibroblasts (NIH 3T3) undergo small volume decrease (<10%) while migrating through

tight spaces, implying limited fluid flow from the nucleus to cytosol(26). This suggests that the dry Poisson's ratio of the nuclei studied here is close to 0.5.

Prediction of lamina buckling and rupture

The NE controls protein trafficking between the cytoplasm and the nucleoplasm and is essential for protecting the chromatin from being exposed to the cytoplasm. Recently it has been shown that rupture of the NE during cell migration through rigid constrictions can potentially lead to herniation of chromatin across the NE and breaking of DNA double strands (13, 14). The rupture and blebs are often found at defective sites in the NE where nuclear lamina signal was weak or absent (14). Interestingly, the occurrences of these events were also associated with the size of the constriction, which influences the degree of nuclear deformation (14). Therefore, we studied the spatial distribution of strains in the NE and predicted possible locations for NE rupture and buckling as the result of large nuclear deformation during transmigration. The in-plane stretch of the NE is inhomogeneous, with the front and back of the lamina being under tension while the side of the nucleus in contact with the gap is under compression (Fig. 3e). As a result, the lamina can rupture in the tensile regions, which in turn can lead to nuclear blebbing (Fig. 3e). Also in the regions that the lamina is under compression, buckling of the NE has been reported previously (14, 26, 35). Using a device to apply controlled compression on the cell, the precise threshold of deformation above which the nuclear lamina ruptures has been found and correlated with the expression of specific sets of genes, including those involved in DNA damage repair (36). From these experimental data (36), we estimated the threshold of in-plane stretch (stretch = 1 + in-plane strain) for NE rupture to be ~1.2. While the cells pass through small gaps, our model predicts a maximal in plane stretch of ~1.3, which exceeds the experimentally measured threshold, indicating the cells are under high risk of NE rupture during transmigration. The in-plane stretch at the front is higher than the stretch at the back (Fig. 3e), suggesting that the front of the nucleus has a higher chance of rupture, which is consistent with recent findings (14) indicating that 70% of NE rupture events occur at the front of the nucleus during the process of cancer cell migration through confined environments (Fig. 3f). As the gap size increases from $0.25r_n$ to $0.5r_n$, the maximum in-plane stretch decreases from 1.3 to 1.1, corresponding to a lower likelihood of NE rupture, which is consistent with the positive correlation between NE rupture and smaller constriction size reported with a microfluidic migration device (14).
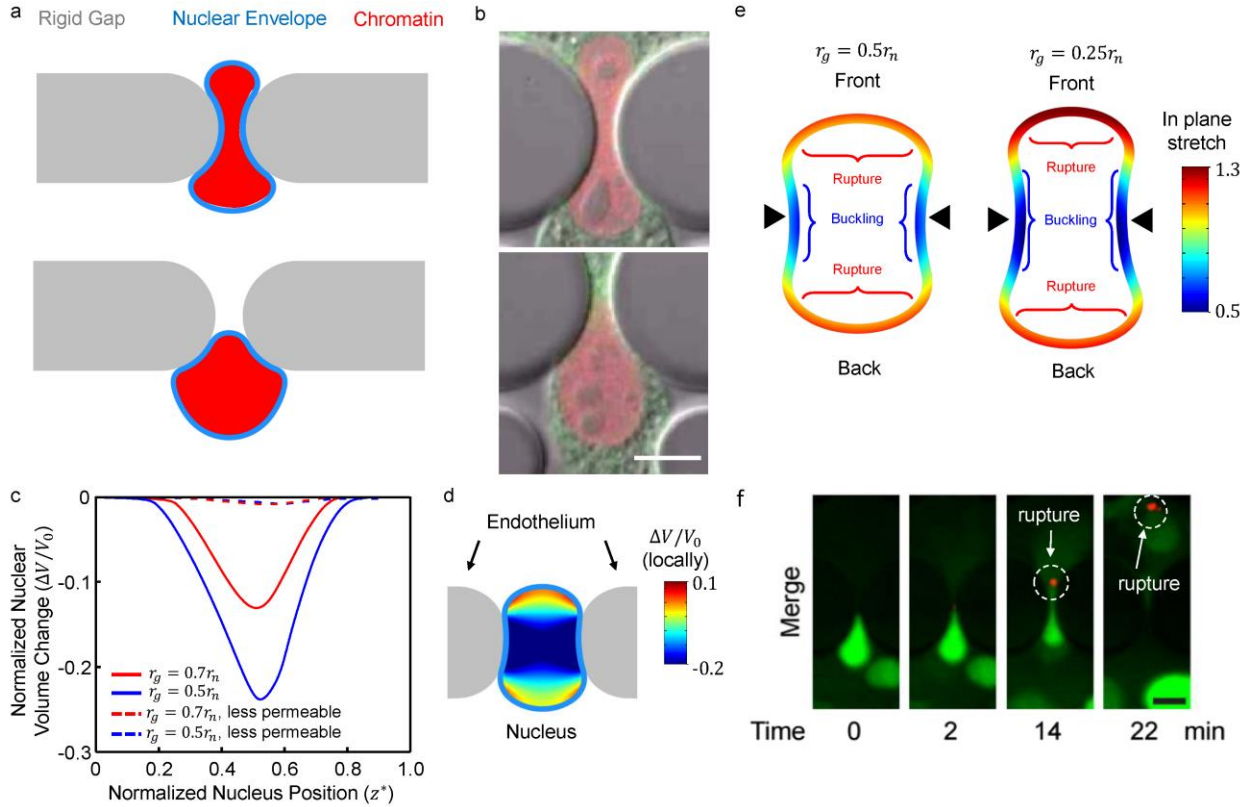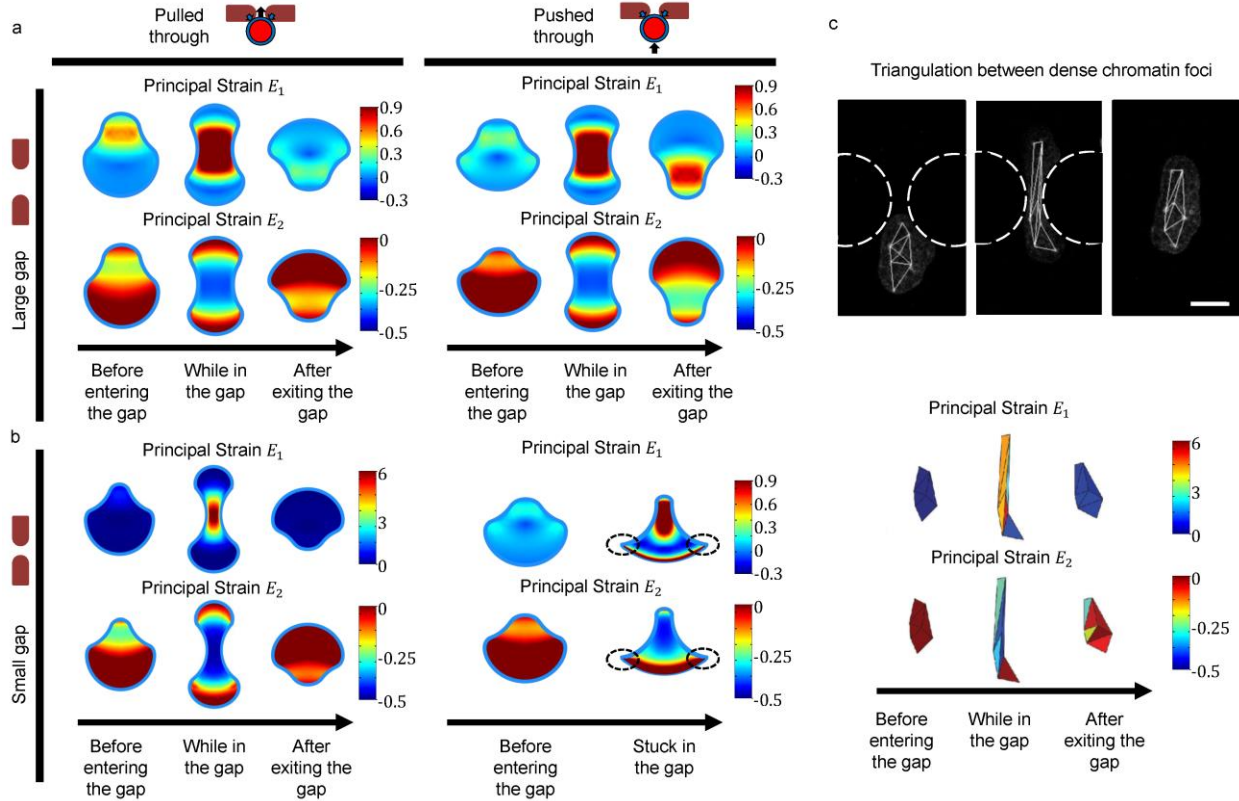
Figure 3: Nuclear shapes, spatial distribution of volumetric strains and fluid content as well as nuclear envelope deformation and rupture: (a) Snapshots of the nuclear shapes at different stages of transmigration through a small rigid gap ($r_g = 0.25r_n$). (b) Nuclear shapes in experiments of cell migration through constrictions in a microfluidic device. The nucleus is labeled by mCherry-Histone4 (red), the cytoplasm by GFP-actin (green). Scale bar, 10 μm. (c) The normalized nuclear volume change ($\Delta V/V_0$) as a function of nuclear position. The nucleus experiences large volumetric strains due to fluid expulsion when it passes through smaller gaps. The model predicts up to ~24% decrease in nuclear volume during transmigration for the smallest gap ($r_g = 0.5r_n$). Also the effect of nuclear permeability on volume change is shown. (d) The local volume change (dilatation) exhibits large spatial variations within the nucleus. Contours show the normalized local volumetric strain for a permeable nucleus passing through a gap size of $r_g = 0.7r_n$ (red line in (c)), with blue representing regions with large volume decrease. (e) In-plane stretch just before the nucleus exits the endothelial gap for: $r_g = 0.5r_n$ (left) and $r_g = 0.25r_n$ (right) (only the NE is shown). The in-plane stretch of the NE is inhomogeneous, with the front and back of the lamina being under tension (potential location of lamina rupture and bleb formation) while the side of the nucleus in contact with the gap is under compression (potential locations for lamina buckling). Black triangles indicate the gap center. (f) Representative time-lapse images showing NE rupture at the front of an HT1080 cell passing through a constriction. The NE rupture was visualized by the spill of NLS-GFP (green) into the cytoplasm and the accumulation of the cytoplasmic DNA binding protein cGAS-RFP (red) at the site of rupture at the NE. Scale bar, 10 μm. Model parameters for (a), (c), (d) and (e) are $K = 1$ kPa, $\rho_0 = 0.5$ kPa, $\beta = 2.77 \times 10^{-3}$ Pa, $\mu_n = 5$ kPa, $\mu_t = 5$ kPa, $\mu_e = 10$ kPa.

Pulling forces as the primary mechanism of transmigration

A recent study identified cortical actin filaments at the back of the cell that can generate pushing forces at the rear of the nucleus that may facilitate transmigration (37). To investigate the role of forces acting on the rear of the nucleus, we dissect the influence of push and pull forces and tested whether push forces acting on the rear of the nucleus can explain the shape and distribution of strain during transmigration. We estimated the maximal (E_1) and the minimal (E_2) principal strains while mapping them at different stages of transmigration through rigid constrictions of different sizes (Fig.4a). Also we considered the cases of either having purely pushing forces at the rear of the nucleus or pulling forces on the front (Fig. 4a and b). For all cases we found that E_1 is mostly in the direction of transmigration, while E_2 is approximately aligned perpendicular to the transmigration direction.

For a relatively large constriction, we find that the nucleus adopts an hourglass shape whether it is pulled by frontal actomyosin forces or pushed by rear cytosolic forces (Fig. 4a). This hourglass shape has been observed in various cell migration experiments (8, 14, 26, 38). Interestingly our model predicts that E_1 and E_2 are mostly tensile and compressive, respectively, consistent with the experimental patterns of strain maps derived based on the triangulation between the individual naturally-present dense chromatin foci (Fig. 4c) (26). However for a smaller constriction, the nucleus still adopts an hourglass shape when it is pulled through, while the pushing at its rear results in an inverted bolt shape (Fig. 4b) and appearance of large compressive E_1 that has not been observed in the experiments (Fig. 4b). Furthermore in the case of small gaps, our simulations suggest that purely pushing forces cannot lead to a successful transmigration and the nucleus remains stuck in the gap. Therefore, pulling from actomyosin forces at the front of the nucleus appears to be the primary driving mechanism of transmigration, particularly for small constrictions.
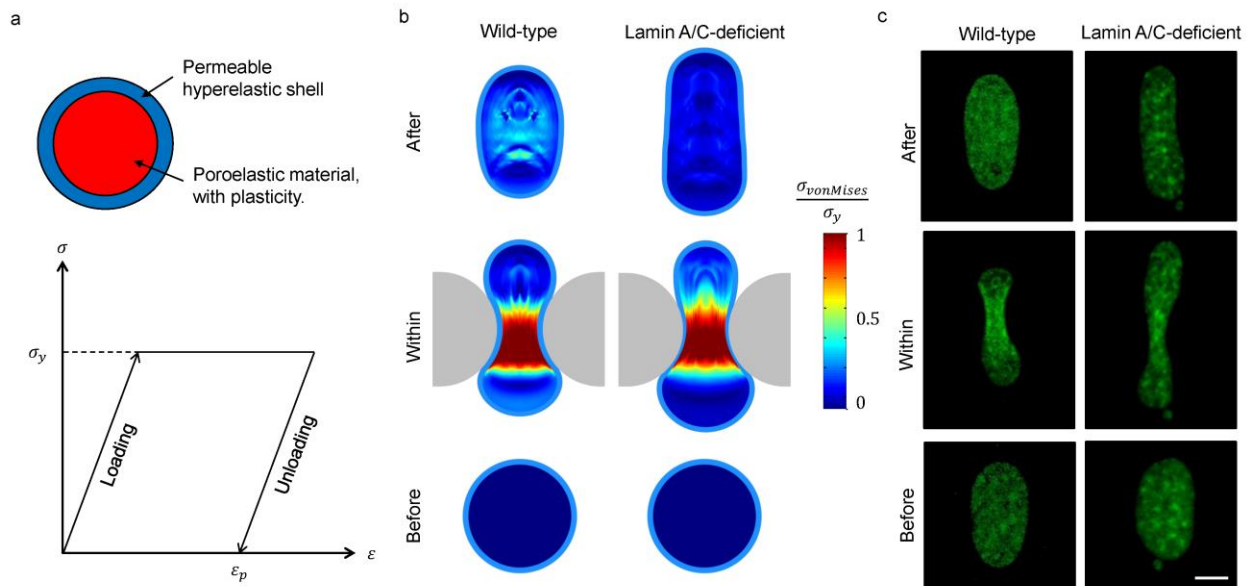
Figure 4: Nuclear strains during transmigration. (a, b) Graphical representation of spatial distributions of strains in the nucleus at different stages of transmigration through large (a) ($r_g = 0.5r_n$) and small (b) ($r_g = 0.25r_n$) rigid constrictions under either pushing (left) or pulling (right) forces. (c) The experimental strain maps of lamin A/C-deficient cells (bottom) based on triangulation between present dense chromatin foci (top). Scale bar, 10 μm. Model parameters are $K = 1$ kPa, $\rho_0 = 0.5$ kPa, $\beta = 2.77 \times 10^{-3}$ Pa, $\mu_n = 5$ kPa, $\mu_t = 5$ kPa.

Effects of plasticity on irreversible nuclear deformations

Previously, Pajerowski et al. reported that cell nuclei experience irreversible deformation after release of pressure applied by a micropipette (16). A later study showed evidence that dynamic loading of the nucleus can lead to permanent structural changes in chromatin (39). Since these studies indicate the existence of significant plastic nuclear deformations, we studied the plastic behavior of the nucleus by treating the filled material (representing the chromatin) as an ideal plastic material (which is the extreme limit of a shear thinning material), with no strain hardening after yielding (Fig. 5a) and the NE is treated as a permeable hyper elastic shell. An ideal plastic material shows elastic response when the stress is below the yield stress; it undergoes plastic (permanent) deformation without any increase in stresses beyond the yield stress (note that we ignored the effect of hydrostatic pressure on plastic flow since it does not influence the qualitative trends). The representative nuclear shapes together with the contour plots of the normalized von-Mises stress (with respect to the yield stress, σ_y) during transmigration through a relative small rigid constriction ($r_g = 0.4r_n$) are shown in Fig. 5b, left panel. Due to the presences of stresses

that exceed the yield stress, the interior of the nucleus undergoes plastic deformation while the elastic properties of the NE still work towards restoring nuclear shape, leading to a permanent prolate ellipsoid shape after exiting the constriction, which is very similar to experimental observations (Fig. 5c, left panel). This conflict between the respective elastic and plastic deformations of the NE and the chromatin results in an inhomogeneous residual stress within the nuclear interior following complete transmigration (Fig. 5b, left panel).

Experimentally it has been shown that the nuclei of cells lacking lamin A/C exhibit larger irreversible shape changes after moving through tight spaces (26, 33) (Fig. 5c, right panel). To capture effects of lamin A/C deficiency on plastic deformation and final shape of the nucleus, we considered a compliant NE that is significantly softer (90% softer, Fig. 5b, right panel) than the control, which represents the wild-type NE with normal levels of lamin A/C (Fig. 5b, left panel). The nuclei of lamin A/C-deficient cells undergo much larger irreversible deformation with significantly larger nuclear aspect ratio of 2.06 compared to wild-type cells with the aspect ratio of 1.52 (Fig.5b, left and right panels). Due to the softer NE, the residual stress within the chromatin decreases and shows a more homogenous distribution after the cell fully exits the constriction compared to wild-type cells. These predictions from our model are in an excellent agreement with our experimental data (Fig 5c) indicating that following transmigration the nuclear aspect ratio increases by ~2.2=3.78/1.74 fold (where 3.78 is the aspect ratio before and 1.74 after transmigration) for the case of lamin A/C-deficient cells that is significantly larger than that of wild-type cell (~1.15=2.12/1.85 fold increase). Taken together our model predictions confirm that lamin A/C regulates nuclear deformability and that nuclei lacking lamin A/C are more plastic and undergo larger irreversible deformation than nuclei from wild-type cells.

Figure 5: Impact of chromatin plasticity and lamina stiffness on nuclear shapes after

transmigration. (a, b) The nucleus changes its shape from a spheroid to prolate ellipsoid during transmigration when plastic nuclear matter is considered. (a) Chromatin is assumed to be ideally plastic, with no strain hardening after yielding. The stress-strain response of the chromatin is shown in the bottom panel. (b) Normalized von-Mises stresses (measured relative to the yield stress (σ_y)) of the nuclear matter during transmigration through a rigid constriction for wild-type (left) and lamin A/C-deficient (right) cells. Due to the presences of stresses that exceed the yield stress, the nucleus undergoes plastic deformation leading to permanent change in shape after exiting the constriction. Lamin A/C deficient cells undergo larger irreversible shape change than wild-type cells. Model parameters: $\mu_n = 5$ kPa, $r_g = 0.4r_n$. (c) Representative nuclear shapes during different stages of transmigration for wild-type (left) and lamin A/C-deficient (right) cells indicating larger irreversible nuclear shape change for lamin A/C-deficient cells compared to wild-type controls, consistent with the simulations. The nucleus is labeled by H2B-mNeon (green). Scale bar, 10 μm.

Discussion

Focusing on nuclear mechanics, we studied the ability of cells to pass through tight interstitial spaces depending on the mechanical and geometrical features of the cell and the extracellular environment with a chemo-mechanical model. We predicted that cells transmigrate more easily with a stiff ECM and large endothelial/constriction gap (Fig. 2c) and estimated the minimal actomyosin contraction force required for transmigration of the nucleus. Indeed, recent experiments suggest that the cells are not able to transmigrate either when contractility (40, 41) is abolished or when nesprin links (41) and/or integrins (4) are inhibited. Cells also deform the endothelium and create larger opening to facilitate transmigration (Supplementary Fig. 5), which implicates that the endothelial cells around the opening are under compression, leading to rupture of cell-cell adhesions within the endothelium. We also quantitatively investigated the influence of transmigration on cell nuclei including nuclear shapes, chromatin deformations and nuclear envelope deformations. Our results predict nuclear shape profiles that closely agree with both our experimental observations and previously published data (8, 14, 26). Furthermore, investigating the nuclear profiles and the distribution of strain within the nucleus, we conclude that the primary driving forces (particularly for transmigration through small gaps) are those that pull the nucleus from the front. This is consistent with the experimental observations of dense regions of actin at the leading edge of cell protrusions extending into the sub-endothelial ECM during tumor cell extravasation (4). Considering plasticity associated with chromatin structure (39) we captured the effects of irreversible nuclear shape changes (Fig. 5) and verified recent observations suggesting that cells lacking lamin A/C are more deformable and undergo more plastic deformations (33).

Our model further predicted that transmigration places extensive physical stress on the nucleus and the NE, particularly at the leading edge, and that the in-plane stretch of the NE can exceed the critical stretch value of ~1.2, placing cells at high risk of NE rupture during transmigration. A major function of the NE is to act as a barrier separating chromatin from the cytoplasm, with nucleo-cytoplasmic exchange closely controlled by the nuclear pore complex. Transmigration

induced rupture of the NE exposes the genomic DNA to normally cytoplasmic factors (Fig. 3f), including nucleases, which could result in DNA damage, as observed in recent studies (13, 14). While cells in those studies were generally able to tolerate NE rupture and DNA damage, combined inhibition of ESCRT-III mediated NE repair and DNA damage repair pathways substantially increased the rate of cell death during transmigration (13, 14), highlighting the importance of maintaining NE integrity during migration. Importantly, some cells also exhibit DNA damage during transmigration through small constrictions even without NE rupture (13). In these cases, DNA damage could result from mechanical straining of the chromatin and/or from volume changes of the nucleus. Our model and experimental data indicate that the nucleus undergoes significant shape changes during transmigration (Fig. 3a), associated with large intranuclear strains (Fig. 4) that impose substantial mechanical stress on the chromatin, which may be sufficient to induce DNA damage. Nuclear volume changes and (local) efflux of water and soluble nuclear components could further contribute to DNA damage. A previous study found that loss of DNA repair enzymes can potentially lead to irreversible DNA damage (42). These enzymes are small molecules and their activity is highly dependent on the distribution and the amount of water accessible to them within the nucleus. Our model predicts an overall volume decrease of up to 24%, which could be sufficient to induce DNA damage by water redistribution and the local loss of DNA repair enzymes.

Our model provides support for the existence of all three mechanisms, which could occur alone or in combination. Currently, the relative contribution of NE rupture, chromatin strain, and nuclear volume change for DNA damage incurred during transmigration remains unclear. Predictions from our model regarding the expected localization of DNA damage, depending on the specific DNA damage mechanism, may be used in combination with quantitative, high resolution time-lapse imaging experiments to fully elucidate the molecular and biophysical details of DNA damage during transmigration.

While these observations pertain specifically to tumor cell transendothelial migration, they are widely applicable to any situation in which a cell needs to pass through narrow constrictions, such as during migration through interstitial spaces (typically ranging from $2 - 20$ μm). Note, however, that in the current simulations, the monolayer gap size at zero stress is taken as fixed, whereas in the case of the endothelial monolayer, it will vary with the degree to which cell-cell adhesions rupture due to the forces generated during transmigration. Nonetheless, in the particular case of TEM, these findings may have important implications with respect to the tendency of tumor cells to survive and proliferate once they extravasate into tissue from the vascular system. Studies are therefore needed to investigate changes in phenotype of cells that have undergone TEM.

Conclusion

In summary, we proposed a model for cell transmigration that provides testable predictions, which are in accord with our experiments and existing literature. The model addresses key factors such as nuclear shape change and nuclear strain, which are crucial to determine the ability of cancer cells to invade and move through the surrounding matrix and which may also help predict the anticipated extent of DNA damage. By tuning the model parameters, our simulations can be adapted to understand cell transmigration for other cells and matrix systems. This work therefore provides a framework to assess the roles of mechanical and geometric features on cell migration across monolayers and through 3D matrices.

Author contributions

X.C., X.W. and V.B.S. formulated the mathematical framework for the chemo-mechanical model; X.C. carried out the computations; E. M., P.I., P.M.D., M.B.C., J.L. and R.D.K. designed the experiments. E.M., P.I., P.M.D. and M.B.C. conducted the experiments. All authors interpreted the data and wrote the manuscript.

References

1.   Reymond, N., B.B. d'Água, and A.J. Ridley. 2013. Crossing the endothelial barrier during metastasis. Nat. Rev. Cancer. 13: 858–70.

2.   Madsen, C.D., and E. Sahai. 2010. Cancer dissemination--lessons from leukocytes. Dev. Cell. 19: 13–26.

3.   Chen, M.B., J.A. Whisler, J.S. Jeon, and R.D. Kamm. 2013. Mechanisms of tumor cell extravasation in an in vitro microvascular network platform. Integr. Biol. (Camb). 5: 1262–71.

4.   Chen, M.B., J.M. Lamar, R. Li, R.O. Hynes, and R.D. Kamm. 2016. Elucidation of the

Roles of Tumor Integrin β1 in the Extravasation Stage of the Metastasis Cascade. Cancer Res. 76: 2513–24.

5.   Friedl, P., K. Wolf, and J. Lammerding. 2011. Nuclear mechanics during cell migration. Curr. Opin. Cell Biol. 23: 55–64.

6.   Moeendarbary, E., L. Valon, M. Fritzsche, A.R. Harris, D.A. Moulding, A.J. Thrasher, E. Stride, L. Mahadevan, and G.T. Charras. 2013. The cytoplasm of living cells behaves as a poroelastic material. Nat. Mater. 12: 253–261.

7.   Charras, G., and E. Sahai. 2014. Physical influences of the extracellular environment on cell migration. Nat. Rev. Mol. Cell Biol. 15: 813–24.

8.   Davidson, P.M., C. Denais, M.C. Bakshi, and J. Lammerding. 2014. Nuclear deformability constitutes a rate-limiting step during cell migration in 3-D environments. Cell. Mol. Bioeng. 7: 293–306.

9.   Wolf, K., M. Te Lindert, M. Krause, S. Alexander, J. Te Riet, A.L. Willis, R.M. Hoffman, C.G. Figdor, S.J. Weiss, and P. Friedl. 2013. Physical limits of cell migration: control by ECM space and nuclear deformation and tuning by proteolysis and traction force. J. Cell Biol. 201: 1069–84.

10.   Harada, T., J. Swift, J. Irianto, J.-W. Shin, K.R. Spinler, A. Athirasala, R. Diegmiller, P.C.D.P. Dingal, I.L. Ivanovska, and D.E. Discher. 2014. Nuclear lamin stiffness is a barrier to 3D migration, but softness can limit survival. J. Cell Biol. 204: 669–82.

11.   Friedl, P., K. Wolf, and J. Lammerding. 2011. Nuclear mechanics during cell migration. Curr. Opin. Cell Biol. 23: 55–64.

12.   Davidson, P.M., and J. Lammerding. 2014. Broken nuclei--lamins, nuclear mechanics, and disease. Trends Cell Biol. 24: 247–56.

13.   Raab, M., M. Gentili, H. de Belly, H.R. Thiam, P. Vargas, A.J. Jimenez, F. Lautenschlaeger, R. Voituriez, A.M. Lennon-Duménil, N. Manel, and M. Piel. 2016. ESCRT III repairs nuclear envelope ruptures during cell migration to limit DNA damage and cell death. Science. : aad7611.

14.   Denais, C.M., R.M. Gilbert, P. Isermann, A.L. McGregor, M. te Lindert, B. Weigelin, P.M. Davidson, P. Friedl, K. Wolf, and J. Lammerding. 2016. Nuclear envelope rupture

and repair during cancer cell migration. Science. 352: 353–358.

15. Guilak, F., J.R. Tedrow, and R. Burgkart. 2000. Viscoelastic properties of the cell nucleus. Biochem. Biophys. Res. Commun. 269: 781–6.

16. Pajerowski, J.D., K.N. Dahl, F.L. Zhong, P.J. Sammak, and D.E. Discher. 2007. Physical plasticity of the nucleus in stem cell differentiation. Proc. Natl. Acad. Sci. U. S. A. 104: 15619–24.

17. Fletcher, D.A., and R.D. Mullins. 2010. Cell mechanics and the cytoskeleton. Nature. 463: 485–492.

18. Moeendarbary, E., and A.R. Harris. 2014. Cell mechanics: principles, practices, and prospects. Wiley Interdiscip. Rev. Syst. Biol. Med. 6: 371–388.

19. Janmey, P.A., and C.A. McCulloch. 2007. Cell mechanics: integrating cell responses to mechanical stimuli. Annu. Rev. Biomed. Eng. 9: 1–34.

20. Panorchan, P., B.W. Schafer, D. Wirtz, and Y. Tseng. 2004. Nuclear envelope breakdown requires overcoming the mechanical integrity of the nuclear lamina. J. Biol. Chem. 279: 43462–7.

21. Swift, J., I.L. Ivanovska, A. Buxboim, T. Harada, P.C.D.P. Dingal, J. Pinter, J.D. Pajerowski, K.R. Spinler, J.-W. Shin, M. Tewari, F. Rehfeldt, D.W. Speicher, and D.E. Discher. 2013. Nuclear Lamin-A Scales with Tissue Stiffness and Enhances Matrix-Directed Differentiation. Science. 341: 1240104.

22. Shenoy, V.B., H. Wang, and X. Wang. 2016. A chemo-mechanical free-energy-based approach to model durotaxis and extracellular stiffness-dependent contraction and polarization of cells. Interface Focus. 6: 20150067.

23. Liu, H., J. Wen, Y. Xiao, J. Liu, S. Hopyan, M. Radisic, C.A. Simmons, and Y. Sun. 2014. In situ mechanical characterization of the cell nucleus by atomic force microscopy. ACS Nano. 8: 3821–8.

24. Lin, D.C., E.K. Dimitriadis, and F. Horkay. 2007. Robust strategies for automated AFM force curve analysis--I. Non-adhesive indentation of soft, inhomogeneous materials. J. Biomech. Eng. 129: 430–40.

25. Bilodeau, G.G. 1992. Regular Pyramid Punch Problem. J. Appl. Mech. 59: 519.

26. Davidson, P.M., J. Sliz, P. Isermann, C. Denais, and J. Lammerding. 2015. Design of a microfluidic device to quantify dynamic intra-nuclear deformation during cell migration through confining environments. Integr. Biol. (Camb). 7: 1534–46.

27. Ghibaudo, M., A. Saez, L. Trichet, A. Xayaphoummine, J. Browaeys, P. Silberzan, A. Buguin, and B. Ladoux. 2008. Traction forces and rigidity sensing regulate cell functions. Soft Matter. 4: 1836.

28. Mitrossilis, D., J. Fouchard, A. Guiroy, N. Desprat, N. Rodriguez, B. Fabry, and A. Asnacios. 2009. Single-cell response to stiffness exhibits muscle-like behavior. Proc. Natl. Acad. Sci. U. S. A. 106: 18243–8.

29. Jeon, H., E. Kim, and C.P. Grigoropoulos. 2011. Measurement of contractile forces generated by individual fibroblasts on self-standing fiber scaffolds. Biomed. Microdevices. 13: 107–15.

30. Dahl, K.N., S.M. Kahn, K.L. Wilson, and D.E. Discher. 2004. The nuclear envelope lamina network has elasticity and a compressibility limit suggestive of a molecular shock absorber. J. Cell Sci. 117: 4779–86.

31. Lammerding, J., L.G. Fong, J.Y. Ji, K. Reue, C.L. Stewart, S.G. Young, and R.T. Lee. 2006. Lamins A and C but not lamin B1 regulate nuclear mechanics. J. Biol. Chem. 281: 25768–80.

32. Lammerding, J., P.C. Schulze, T. Takahashi, S. Kozlov, T. Sullivan, R.D. Kamm, C.L. Stewart, and R.T. Lee. 2004. Lamin A/C deficiency causes defective nuclear mechanics and mechanotransduction. J. Clin. Invest. 113: 370–8.

33. Rowat, A.C., D.E. Jaalouk, M. Zwerger, W.L. Ung, I.A. Eydelnant, D.E. Olins, A.L. Olins, H. Herrmann, D.A. Weitz, and J. Lammerding. 2013. Nuclear envelope composition determines the ability of neutrophil-type cells to passage through micron-scale constrictions. J. Biol. Chem. 288: 8610–8.

34. Salbreux, G., G. Charras, and E. Paluch. 2012. Actin cortex mechanics and cellular morphogenesis. Trends Cell Biol. 22: 536–45.

35. Kim, D.-H., B. Li, F. Si, J.M. Phillip, D. Wirtz, and S.X. Sun. 2015. Volume regulation

and shape bifurcation in the cell nucleus. J. Cell Sci. 128: 3375–85.

36. Le Berre, M., J. Aubertin, and M. Piel. 2012. Fine control of nuclear confinement identifies a threshold deformation leading to lamina rupture and induction of specific genes. Integr. Biol. (Camb). 4: 1406–14.

37. Norden, C., S. Young, B.A. Link, and W.A. Harris. 2009. Actomyosin is the main driver of interkinetic nuclear migration in the retina. Cell. 138: 1195–208.

38. Kim, M.-C., D.M. Neal, R.D. Kamm, and H.H. Asada. 2013. Dynamic modeling of cell migration and spreading behaviors on fibronectin coated planar substrates and micropatterned geometries. PLoS Comput. Biol. 9: e1002926.

39. Poh, Y.-C., S.P. Shevtsov, F. Chowdhury, D.C. Wu, S. Na, M. Dundr, and N. Wang. 2012. Dynamic force-induced direct dissociation of protein complexes in a nuclear body in living cells. Nat. Commun. 3: 866.

40. Stoletov, K., H. Kato, E. Zardouzian, J. Kelber, J. Yang, S. Shattil, and R. Klemke. 2010. Visualizing extravasation dynamics of metastatic tumor cells. J. Cell Sci. 123: 2332–41.

41. Thomas, D.G., A. Yenepalli, C.M. Denais, A. Rape, J.R. Beach, Y. -l. Wang, W.P. Schiemann, H. Baskaran, J. Lammerding, and T.T. Egelhoff. 2015. Non-muscle myosin IIB is critical for nuclear translocation during 3D invasion. J. Cell Biol. 210: 583–594.

42. Karschau, J., C. de Almeida, M.C. Richard, S. Miller, I.R. Booth, C. Grebogi, and A.P.S. de Moura. 2011. A matter of life or death: modeling DNA damage and repair in bacteria. Biophys. J. 100: 814–21.

43. Fawcett, D.W. 1966. On the occurrence of a fibrous lamina on the inner aspect of the nuclear envelope in certain cells of vertebrates. Am. J. Anat. 119: 129–45.

44. Hall, M. 1975. Bulk modulus of a fluid−filled spherical shell. J. Acoust. Soc. Am. 57: 508.

45. Gerlitz, G., and M. Bustin. 2010. Efficient cell migration requires global chromatin condensation. J. Cell Sci. 123: 2207–17.

46. Century, T.J., I.R. Fenichel, and S.B. Horowitz. 1970. The Concentrations of Water,

Sodium and Potassium in the Nucleus and Cytoplasm of Amphibian Oocytes. J. Cell Sci. 7: 5–13.

47.   Abu-Arish, A., P. Kalab, J. Ng-Kamstra, K. Weis, and C. Fradin. 2009. Spatial distribution and mobility of the Ran GTPase in live interphase cells. Biophys. J. 97: 2164–78.

48.   Caille, N., O. Thoumine, Y. Tardy, and J.-J. Meister. 2002. Contribution of the nucleus to the mechanical properties of endothelial cells. J. Biomech. 35: 177–87.

49.   Zeng, D., T. Juzkiw, A.T. Read, D.W.-H. Chan, M.R. Glucksberg, C.R. Ethier, and M. Johnson. 2010. Young's modulus of elasticity of Schlemm's canal endothelial cells. Biomech. Model. Mechanobiol. 9: 19–33.

50.   Thomasy, S.M., V.K. Raghunathan, M. Winkler, C.M. Reilly, A.R. Sadeli, P. Russell, J. V Jester, and C.J. Murphy. 2014. Elastic modulus and collagen organization of the rabbit cornea: epithelium to endothelium. Acta Biomater. 10: 785–91.

51.   Chiron, S., C. Tomczak, A. Duperray, J. Lainé, G. Bonne, A. Eder, A. Hansen, T. Eschenhagen, C. Verdier, and C. Coirault. 2012. Complex interactions between human myoblasts and the surrounding 3D fibrin-based matrix. PLoS One. 7: e36173.

52.   Wang, H., A.A. Svoronos, T. Boudou, M.S. Sakar, J.Y. Schell, J.R. Morgan, C.S. Chen, and V.B. Shenoy. 2013. Necking and failure of constrained 3D microtissues induced by cellular tension. Proc. Natl. Acad. Sci. U. S. A. 110: 20923–8.

53.   Pellegrin, S., and H. Mellor. 2007. Actin stress fibres. J. Cell Sci. 120: 3491–9.

54.   Sawada, Y., M. Tamada, B.J. Dubin-Thaler, O. Cherniavskaya, R. Sakai, S. Tanaka, and M.P. Sheetz. 2006. Force sensing by mechanical extension of the Src family kinase substrate p130Cas. Cell. 127: 1015–26.

55.   Puklin-Faucher, E., and M.P. Sheetz. 2009. The mechanical integrin cycle. J. Cell Sci. 122: 179–86.

56.   Katoh, K., Y. Kano, M. Amano, H. Onishi, K. Kaibuchi, and K. Fujiwara. 2001. Rho-Kinase–Mediated Contraction of Isolated Stress Fibers. J. Cell Biol. 153: 569–584.

57.   Matthews, B.D., C.K. Thodeti, J.D. Tytell, A. Mammoto, D.R. Overby, and D.E. Ingber. 2010. Ultra-rapid activation of TRPV4 ion channels by mechanical forces applied to cell surface beta1 integrins. Integr. Biol. (Camb). 2: 435–42.

Supplementary Information

Chemo-mechanical model for cell transmigration through small interstitial spaces.

 (a) Model for the mechanical response of the nucleus.
The nucleus is the stiffest compartment within the cell and becomes the limiting factor in transmigration. Recently, Kim et al. used a non-linear shell model to analyze the mechanics of the nucleus. The shell represents the nuclear envelope (NE)(35), treated as a hyperelastic material obeying a neo-Hookean constitutive relationship. This approach was shown to be reasonable since it captures the shape and size of the nucleus when subjects to mechanical and osmotic loads. Following a similar approach, we treat the nucleus as a hyperelastic shell following a neo-Hookean constitutive relationship (with shear modulus μ_s and Poisson's ratio 0.3). The NEs mainly consist of lamins(43), the lamin A/C concentration within the NE has been shown to greatly impact on the deformability of the nucleus(33), as well as in the regulation of cell migration and differentiation(10, 21), These findings indicate that the thin NE dominates the mechanical response of the nucleus. We assume the NE has a shear modulus of $\mu_s = (r_n/h)\mu_n$, where μ_n is the shear modulus of the nucleus, and h is set as $h = 0.1r_n$ to ensure the NE is relative thin. Since bulk modulus is linearly correlated with shear modulus, the effective bulk modulus(44) of the nuclear model used here is $\kappa_{eff} = (h/r_n)\,\kappa_s = \kappa_n$. Therefore, this setup ensures that the "effective" bulk modulus that relates pressure to the overall volume change is comparable to the measurements from micropipette aspiration experiments.

We also considered the mechanical response of chromatin and other structures that are encased in the NE, which was ignored in Kim's model. A recent study reported that large chromatin condensation (~2 fold) is required for efficient cell migration, especially through small pores(45). Considering the high volume of water (~80%) contained within the nucleus(46), the chromatin and other sub-cellular structures within the nucleus are treated as a soft poroelastic material with shear modulus $\mu_c = 0.1\mu_n$ and the 'dry' Poisson's ratio 0.3. Though the NE is directly permeable to water, the transport of other molecules is regulated(47), which can be addressed by assigning different 'dry' Poisson's ratios (to be discussed later). The characteristic time for the fluid within the nucleus to flow out of the nucleus in response to the compressive forces it experiences during transmigration can be estimated as $\tau = r_n^2/D_c$, where D_c is the poroelastic diffusion coefficient and r_n is the radius of the nucleus. Using the parameters reported in the literature $(r_n{\sim}3\mu m, D_c{\sim}50\mu m^2/s)$(6), the characteristic time for water to flow out of the nucleus is found

to be ~0.18s, which is much faster than the time it takes for of transmigration (~15 minutes to few hours)(3). Here we only focus on the steady state shape, where the water flow has ceased. The high concentration of charged chromatin inside the nucleus also suggests that the osmotic pressure across the NE is unequal. In cells adhered to substrates, the difference in the osmotic pressure has been shown to be approximately $10^{-2}\,\mu_n$ (μ_n is the shear modulus of the nucleus) (35), whereas the computed stresses in the shell when the nucleus squeezes through small gaps is of order $0.1 - 1\,\mu_n$. Therefore, we did not include the osmotic pressure in our model. To summarize, we assume that the nucleus has a stiff shell to represent the NE and is filled with a softer poroelastic material to represent chromatin as shown in Fig. 1c. The change in the volume of the shell during deformation is due to the outward flux of water (that takes place over a few seconds to minutes, faster than the time it takes for transmigration). The numerical values of all the model parameters used are given in Table S1.

Table S1

List of parameters used in the model

Model Parameter	Description	Typical Value	Source
μ_n	Nuclear shear modulus	~5 kPa	N. Caille, et al. (48)
μ_e	Endothelial shear modulus	~1 – 10 kPa	D. Zeng, et al. (49), S. M. Thomasy, et al. (50)
ν_e	Poisson's ratio for endothelium	0.3	Typical value for compressible neo-Hookean material
μ_t	ECM modulus	~0.05 – 5 kPa	Typical tissue modulus
ν_e	Poisson's ratio for ECM	0.3	Typical value for compressible neo-Hookean material
r_n	Nuclear radius	~1 – 5 µm	Typical nucleus radius
r_g	Endothelial gap radius	~ 0.5 – 5 µm	K. Wolf, et al. (9)
β	Chemo-mechanical coupling parameters related to the molecular mechanisms that regulate the engagement of motors	~ 2.77×10^{-3} Pa	V. Shenoy, et al. (22)
K	Stiffness of the cytoskeleton	~1 kPa	S. Chiron, et al. (51)
ρ_0	Initial myosin motor density	~0.5 kPa	H. Wang, et al. (52)

(b) Model for the ECM and the endothelium or constrictions.
To model extracellular environment for transmigration, we introduce a small gap of radius r_g in the endothelium (or more generally a constriction in a microfluidic device). We describe the mechanical response of the endothelium (or the walls of the constrictions) and the ECM using a compressible neo-Hookean hyperelastic material model (with Poisson's ratio $\nu = 0.3$, which is a typical value for compressible neo-Hookean materials). This model behaves like a linear-elastic model at small strains, and shows strain hardening both in compression and tension, a hallmark of biomaterials. The Cauchy (or true) stress tensor for this model is given by:

$$\boldsymbol{\sigma} = \mu(\boldsymbol{FF}^T - tr(\boldsymbol{FF}^T)/3)/J^{\frac{5}{3}} - \kappa(J - 1) \tag{1}$$

where F is the deformation gradient tensor: $F_{ij} = \partial x_i / \partial X_j$, where nuclear material points in the initial and current configurations are given, respectively by x_i and X_j; $J = \det(F)$ is the determinant of the deformations gradient tensor, which indicates relative volume change of the material elements. Here μ is the small-strain shear modulus of the material, and we assign different shear moduli, μ_e and μ_t to the endothelium (or the material that surrounds the constrictions in microfluidic devices) and the ECM, respectively; κ is the bulk modulus and is related to the small-strain Poisson's ratio through the relation, $\kappa = 2\mu(1 + v)/(1 - 2v)/3$.

(c) Chemo-mechanical description of the stress-fiber network.

It has been reported that actomyosin contraction provides the force necessary for the nucleus to translocate through tight spaces (41). Recent studies with microfluidic devices show increased GFP-actin activity at the front of the cell during migration (Fig. 1a) (3). Therefore, we consider the actin filament contraction at the front as the only driving force for transmigration firstly, while the effect of pushing at the back due to cortex actin will be discussed later. The forces exerted by the actin filaments (connected to the nucleus through the linker of nucleoskeleton and cytoskeleton (LINC complex)) are assumed to be uniformly distributed on the top-side of the nucleus (refer to Fig. 1c). Uniformly distributed forces (same amount but along opposite direction) are acted on the projected region of the nucleus top-side on the ECM. As the nucleus moves through the endothelial gap, as the first approximation we assume that it does not exert any frictional forces, thus all contact forces are assumed to be normal forces. This assumption is justified by comparing the nuclear shapes predicted by our model with the shapes observed in experiments. The actomyosin contractile forces are balanced by the forces (in the opposite sense) exerted on the nucleus by the endothelial layer (Fig. 1c). A mechano-chemical model that accounts for both active (myosin) and passive elastic elements is used to model the actin filaments. As described in our previous study (22), both Rho-ROCK and Ca-pathways control stress-dependent myosin motor recruitment and binding with the cytoskeleton. During transmigration, the stress-fibers apply tensile forces to the molecular complex at the focal adhesions (53) that link them to the ECM, which trigger a variety of biochemical processes. One of these events is the conformation change of Vinculin and p130Cas, exposing binding sites of Src-family kinases (SFKs) (54, 55). SFKs act on Rho-GTPases by controlling the activity of guanine nucleotide exchange factors (GEFs) and GTPase activating proteins (GAPs), and increased activity of Rho promotes Rho kinase (ROCK) mediated phosphorylation of myosin phosphatase targeting protein (MYPT), which ultimately, down-regulates motor unbinding (56). The Ca^{2+} pathway regulates the rapid binding of motors to the cytoskeleton (57). This process includes Ca^{2+} flux into cytoplasm and promotes motor binding with increasing tension acting on the cell membrane. The main outcome of these stress-dependent signaling pathways is that motors switch from inactive states (red in Fig. 1d) to active states (green in Fig. 1d), which causes an increase in the density of force dipoles (representing myosin motors) and alignment in the direction of applied stress.

When the above stress-dependent processes that regulate cell contractility are considered, the contractile stress of the actin filaments can be written (22) as,

$$\sigma = \rho + K\varepsilon$$

and the force exerted by the stress-fibers in transmigration can be written as

$$F_\alpha = \sigma \pi r_n^2 = (\rho + K\varepsilon)\pi r_n^2 \tag{2}$$

where ρ is the density of force-dipoles (representing myosin motors/contractility) in the actin network, ε is the strain of the actin filaments, and K is the effective passive stiffness of the actin filaments. The first and second terms in the equation for σ and F_α denote the active and passive contributions to the force. The contractility itself depends on the mechano-chemical coupling discussed in above and can be written (22) as,

$$\rho = \frac{\beta\rho_0}{\beta-\alpha} + \frac{\alpha K - 1}{\beta-\alpha}\varepsilon \tag{3}$$

where ρ_0 is the contractility in the absence of adhesions, α and β denote mechano-chemical coupling parameters that relate to the molecular mechanisms that regulate the stress-dependent signaling pathways and engagement of motors respectively (refer to Fig. 1d) and satisfy the criterion (22) that $0 < \alpha/\beta < 1$. From Eq. (3), it is clear that the cell generates large contractile forces for large values of the feedback parameter, i.e. $\alpha \to \beta$. Treating the cell with contractility inhibiting drugs effectively reduces the strength of the feedback parameters by down regulating the signaling pathways.

Prior to considering the full 3D analysis of transmigration, in order to illustrate how the contractile force depends on the mechanical properties of the ECM and the nucleus, we consider a simplified 1D model: a contractile element sandwiched between the nucleus and the ECM with K_{ECM}^* and K_n^* denoting the effective stiffness of the ECM and nucleus respectively as shown in Fig. 1e. The strain of actin filaments can be expressed as $\varepsilon = -\Delta l/L$, where Δl is the contraction length of actin filament, L is the initial average length of actin filament (shown in Fig. 1c and e). The contraction length of actin filaments, Δl, can be related to the displacement (strain) of the nucleus and the ECM: $\Delta l = L - l = \Delta l_{ECM} + \Delta l_n$, where Δl_{ECM} and Δl_n are the displacements of the ECM and the nucleus respectively (refer to Fig. 1e). Assuming the ECM and nucleus are linear elastic, we can write,

$$\varepsilon_{ECM} = \frac{\sigma}{K_{ECM}^*}, \varepsilon_n = \frac{\sigma}{K_n^*}$$

Along with geometric boundary condition $\varepsilon + \varepsilon_{ECM} + \varepsilon_n = 0$ and Eq. (3), the stress generated by the contractile element is given as,

$$\sigma = \frac{1}{\frac{1}{K_{eff}} + \frac{(\beta-\alpha)}{K\beta-1}} \frac{\beta\rho_0}{K\beta-1} \tag{4}$$

where $K_{eff} = K_{ECM}^* K_n^*/(K_{ECM}^* + K_n^*)$. The above equation shows that the increasing stiffness of either the ECM or the nucleus leads to an increase in the contractility and hence the net force

exerted by the actin filaments. The maximum level of contractility is achieved when $K_{eff} \to \infty$ and is given by $\beta\rho_0/(\beta - \alpha)$. Having established the stiffness dependence of the contractile force, next we use 3D simulation to determine if it is sufficient to pull the nucleus through the endothelium.

To calculate the deformation of the nucleus, the endothelium and the ECM during transmigration, we implemented the model and the constitutive equations Eq. (1) in the finite element (FEM) package, COMSOL 5.1. The resistance force F depends on the model parameters: 1) μ_n and r_n – shear modulus and radius of the nucleus, 2) μ_e – shear modulus of the endothelium, 3) μ_t – shear modulus of the ECM and 4) r_g – endothelial gap size. In terms of dimensionless parameters, we have

$$F^* = \frac{F}{\mu_n r_n^2} = F^*(\frac{r_g}{r_n}, \frac{\mu_e}{\mu_n}, \frac{\mu_t}{\mu_n}) \tag{5}$$

where we have scaled all length with the nuclear radius r_n and all shear modulus with the shear modulus of the nucleus μ_n. Transmigration can only happen when the driving force provided by actin filaments is larger than the resistance force, $F_\alpha \geq F$. The simulation steps are shown in Supplementary Fig. 1.
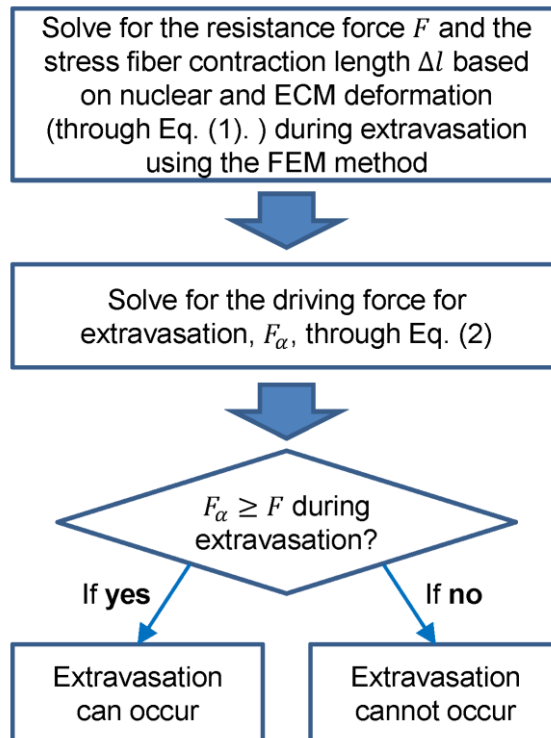

Supplementary Fig. 1: Flowchart depicting the simulation steps.
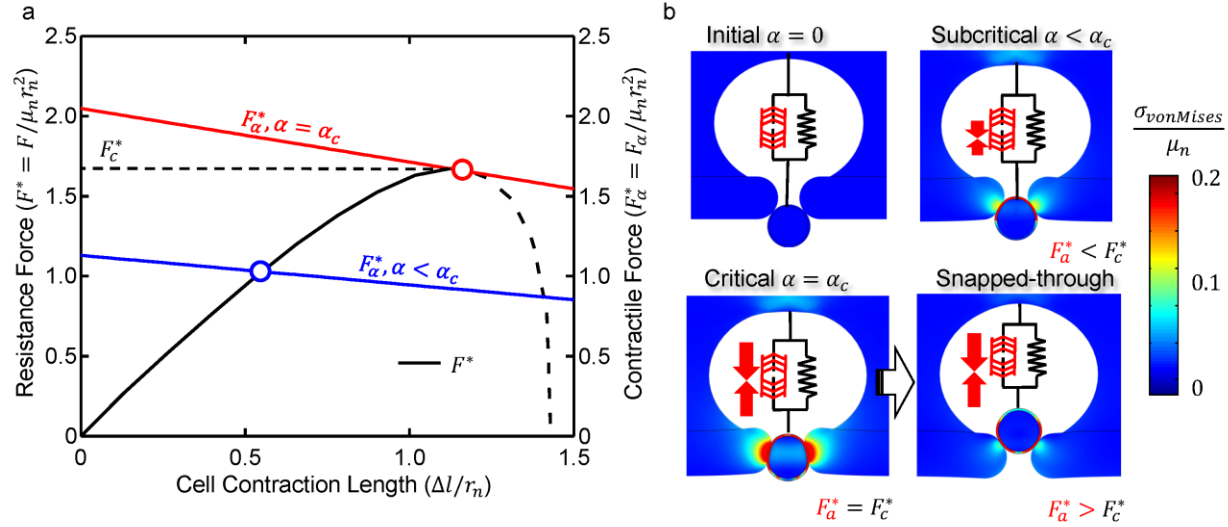
Supplementary Fig. 2: (a) Normalized resistance force (F^*) plotted as a function of the cell contraction length during transmigration for the nucleus (black) as well as normalized contractile force (F_α^*) at different feedback strength levels (blue and red). As the nucleus enters the endothelial gap, the resistance force increases until the nucleus snaps through the gap, leading to a drop in the resistance force (denoted by dashed lines in (a)). Blue is the normalized contractile force from actin filaments at low feedback level, in which case, the cell cannot transmigrate through the endothelium due to lack of driving force (upper panel in (b)). Red is the case at critical feedback level, under which circumstance, the cell is able to build up just enough driving force for transmigration and shows snapped-through behavior (lower panel in (b)). (b) Stress maps in the system: At weak feedback levels, the cell is unable to build up enough driving force for the nucleus to pass through (top panel). At higher feedback level (critical level shown here), the cell is able to generate the critical force required to snap through the endothelial layer. Colors indicate the normalized von-Mises stress (with respect to the nuclear shear modulus) in the system. Model parameters are $\mu_n = 5$ kPa, $\mu_t = \mu_e = 1$ kPa, $r_g = 0.5 r_n$, $r_c = 2.5 r_n$, $K = 1$ kPa, $\rho_0 = 0.5$ kPa, $\beta = 2.77 \times 10^{-3}$ Pa. The critical contractility critical feedback strengths are determined to be $\alpha_c = 2.34 \times 10^{-3}$ Pa.
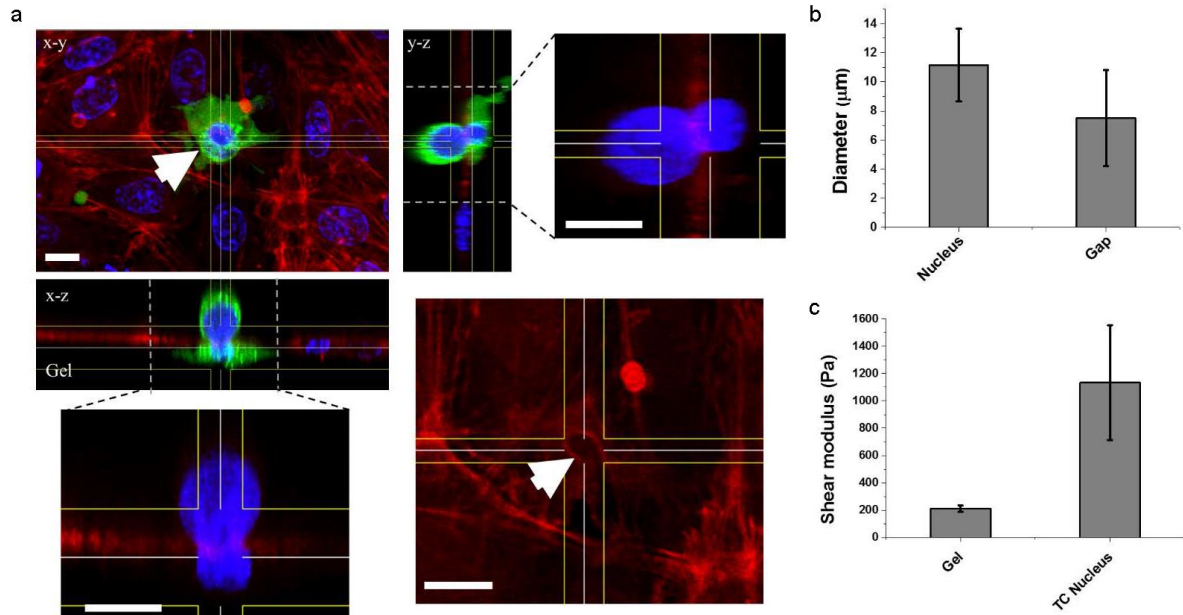
Supplementary Fig. 3: (a) High resolution confocal z-stack of a cancer cell (cytoplasmic-GFP, MDA-MB-231, green) transmigrating through an endothelial monolayer (Lifeact, HUVECs, red) cultured on a collagen gel. The nucleus is stained with Hoechst in blue. Small actin rich ring (white arrowhead) indicates the size of the endothelial opening during transmigration. (b) Average nuclear diameter of the cancer cells prior to transmigration (n=15 cells) and the endothelial opening size (n=8 cells) during transmigration. (c) Shear modulus of the collagen matrix (N=3 gels) and the nucleus of cancer cells (n=15 cells) measured via AFM indentation tests.
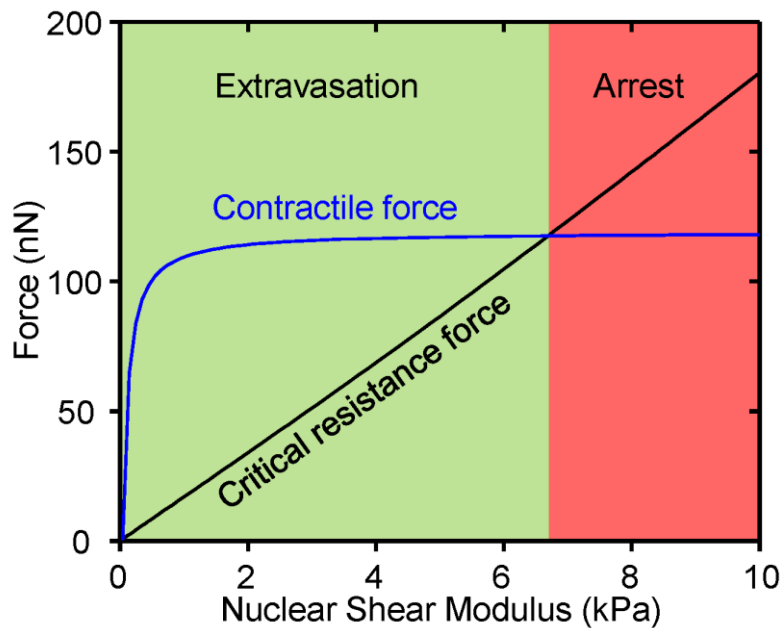

Supplementary Fig. 4: Resistance force (black) and contractile force of the actin filaments (blue) plotted as a function of the nuclear shear modulus. The contractile force of the actin filaments increases with the nuclear modulus. Stiff nuclei are not able to extravasate due to the lack of

sufficiently large contractile forces. Model parameters are $K = 1$ kPa, $\rho_0 = 0.5$ kPa, $\alpha = 2.4 \times 10^{-3}$ Pa, $\beta = 2.77 \times 10^{-3}$ Pa, $\mu_t = 5$ kPa, $\mu_e = 10$ kPa, $r_g = 0.5r_n$.
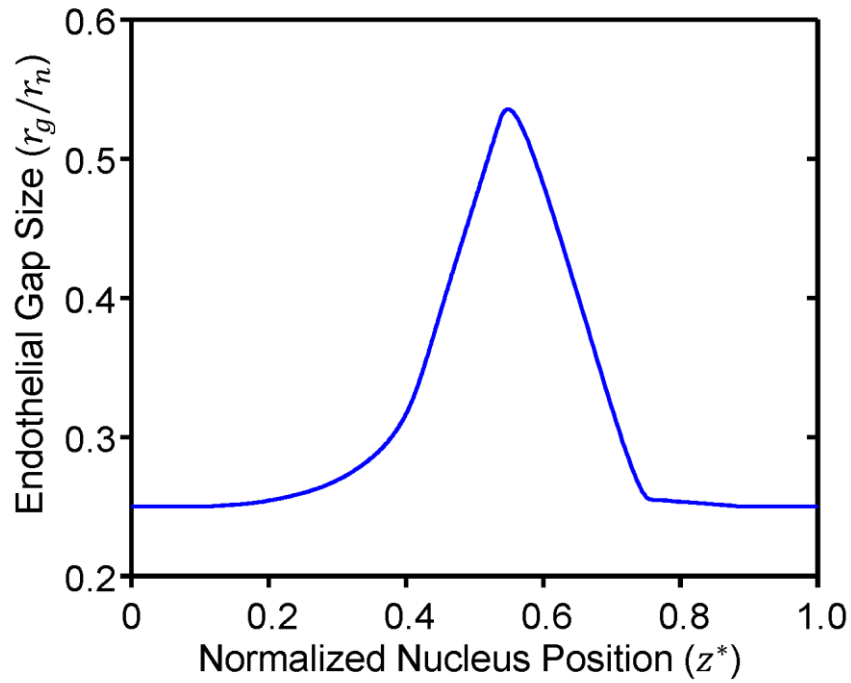
Supplementary Fig. 5: The endothelial gap size changes during transmigration. The forces on the nucleus can lead to an increase in the endothelial gap. It implicates that the endothelial cells around the opening are under compression, leading to rupture of cell-cell adhesions within the endothelium. Model parameters are $K = 1$ kPa, $\rho_0 = 0.5$ kPa, $\alpha = 2.4 \times 10^{-3}$ Pa, $\beta = 2.77 \times 10^{-3}$ Pa, $\mu_n = 5$ kPa, $\mu_t = 5$ kPa, $\mu_e = 10$ kPa, $r_g = 0.25r_n$.
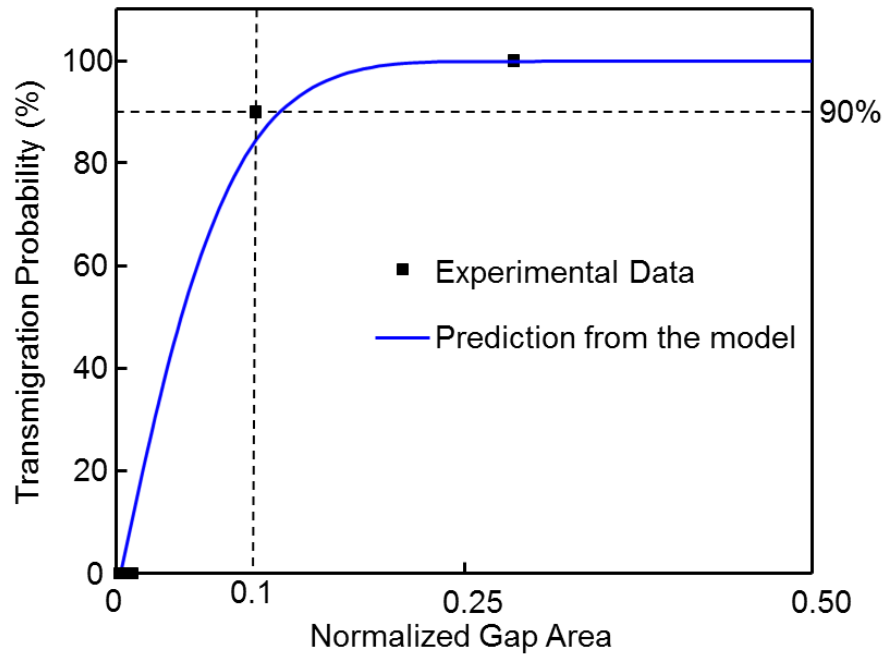
Supplementary Fig. 6: Transmigration probability vs. Normalized gap area (w.r.t cell nuclear cross-section). Model predictions are consistent with experimental results (from K. Wolf et al. (9)): the physical limit of gap size for successful transmigration is 10% of the cross section of the cell nucleus. Model parameters are $K = 1$ kPa, $\rho_0 = 0.5$ kPa, $\alpha = 2.4 \times 10^{-3}$ Pa, $\beta = 2.77 \times 10^{-3}$ Pa, $\mu_n = 5$ kPa, $\mu_t = 5$ kPa, $\mu_e = 10$ kPa.